

## Self-compacting high-performance fiber concrete for foundations

### Part 1 -experimental verification and design considerations

Walraven, Joost; Droogné, Didier; Grünewald, Steffen; Taerwe, Luc; Cotovanu, Bogdan; Rovers, John

**DOI**

[10.1002/suco.202000440](https://doi.org/10.1002/suco.202000440)

**Publication date**

2021

**Document Version**

Final published version

**Published in**

Structural Concrete

**Citation (APA)**

Walraven, J., Droogné, D., Grünewald, S., Taerwe, L., Cotovanu, B., & Rovers, J. (2021). Self-compacting high-performance fiber concrete for foundations: Part 1 -experimental verification and design considerations. *Structural Concrete*, 23(1), 172-186. <https://doi.org/10.1002/suco.202000440>

**Important note**

To cite this publication, please use the final published version (if applicable).  
Please check the document version above.

**Copyright**


Other than for strictly personal use, it is not permitted to download, forward or distribute the text or part of it, without the consent of the author(s) and/or copyright holder(s), unless the work is under an open content license such as Creative Commons.

**Takedown policy**

Please contact us and provide details if you believe this document breaches copyrights.  
We will remove access to the work immediately and investigate your claim.

## ARTICLE

# Self-compacting high-performance fiber concrete for foundations: Part 1 -experimental verification and design considerations

Joost Walraven<sup>1</sup>  | Didier Droogné<sup>2</sup> | Steffen Grünewald<sup>1,2</sup> | Luc Taerwe<sup>2,3</sup> | Bogdan Cotovanu<sup>4</sup> | John Rovers<sup>4</sup>

<sup>1</sup>Faculty of Civil Engineering and Geosciences, Delft University of Technology, Delft, The Netherlands

<sup>2</sup>Department of Structural Engineering and Building Materials, Ghent University, Ghent, Belgium

<sup>3</sup>College of Civil Engineering, Tongji University, Shanghai, China

<sup>4</sup>Department Shell Global Solutions, Shell, Rijswijk, The Netherlands

## Correspondence

Joost Walraven, Faculty of Civil Engineering, Delft University of Technology, Delft, The Netherlands.  
Email: jcw@tudelft.nl

## Abstract

An investigation is carried out into the applicability of self-compacting high-performance fiber concrete (HPFC) in foundations. A concrete mixture has been designed with a concrete cube strength of about 110 MPa. The concrete contains 60 kg/m<sup>3</sup> steel fibers. The properties of the HPFC developed are very suitable for structural applications, especially because the post-cracking tensile strength, provided by the fibers, is higher than the axial tensile strength of the concrete so that hardening in tension occurs after crack formation, often characterized by multiple cracking. This not only results in a high bearing capacity but as well in substantial durability. As a potential application foundation elements are considered. Experiments have been carried out to determine the pre- and post-cracking strength properties, the shear resistance of short beams with loads near to the supports, the anchorage length of reinforcing bars, and the shear capacity of pile caps. The results of the tests are used for verification of the applicability of the general design rules for fiber concrete, as found in the *fib* Model Code 2010, to the HPFC developed. The HPFC developed is characterized by high strength and ductility, is durable and self-compacting. The research program showed that the design of structures with the HPFC considered can be based on existing design rules with some extensions.

## KEYWORDS

design recommendation, experiments, foundations, high performance fiber concrete, sustainable and durable

Discussion on this paper must be submitted within two months of the print publication. The discussion will then be published in print, along with the authors' closure, if any, approximately nine months after the print publication.

This is an open access article under the terms of the Creative Commons Attribution License, which permits use, distribution and reproduction in any medium, provided the original work is properly cited.

© 2021 The Authors. *Structural Concrete* published by John Wiley & Sons Ltd on behalf of International Federation for Structural Concrete

## 1 | INTRODUCTION

The history of fiber reinforced concrete is remarkable. The development of fiber reinforced concrete with a compressive strength in the range C25/30, with a fiber content of about 30–60 kg/m<sup>3</sup>, more or less stabilized in the

90s. Large-scale applications were realized in industrial floors and underwater slabs, but a definite break true of this traditional fiber concrete was not realized. However, at the beginning of the 21st century, the material ultra-high-performance concrete (UHPC) was introduced. This new type of fiber concrete with a compressive strength in the range of 150–200 MPa material was a revolutionary step ahead in the development of fiber concrete. The new material UHPC was a result of a new way of thinking: reduce the maximum particle size to avoid large local stresses in the concrete, optimize the particle packing density (Figure 1), ensure that all water in the concrete is used for hydration and use the remaining unhydrated cement particles as fillers, and add steel fibers to make the material not only strong but also ductile. In *fib* a new Task Group on UHPC was installed, additional to the existing Task Group “Fibre Reinforced Concrete,” with the aim to develop a design guideline for this new promising material. However, this could have resulted in separate design recommendations for conventional FRC and UHPC. This would mean that an intermediate area would remain between the traditional and the new ultra-high-strength fiber concrete, for which no design rules would be available. This area, however, offers as well very interesting opportunities. The production costs of an “intermediate fiber concrete” are significantly lower than those of UHPC, but its properties would make this material suitable for interesting new applications, like instance bridge decks, or prestressed concrete sheet piles.

In order not to “forget” the intermediate range of fiber concretes the *fib* Model Code 2010<sup>2,3</sup> was extended with a part on fiber reinforced concrete, covering the full range from C25 to C200. The present paper intends to

show that the “intermediate range” indeed hosts fiber concretes with a high potential for successful application. It shows that it is possible to “design” a concrete for required properties, with regard to strength, ductility, durability, and self-compactability and as such realize tailor-made applications.

The concrete treated in this paper has especially been designed for its application in foundations. Those structural elements are mostly massive and contain a substantial volume of reinforcement (Figure 2). The idea was to develop concrete that is self-compacting, so that the labor at the building site is reduced, and construction time is shortened. Moreover, it should have strength and ductility properties that guarantee a substantial reduction of the volume of both concrete and reinforcement. But first of all, it should be verified whether such structures can be realized using existing codes, possibly with small modifications. For this purpose, a number of tests have been carried out.

## 2 | DETERMINATION OF THE PROPERTIES OF A SELF-COMPACTING HIGH-PERFORMANCE FIBER REINFORCED CONCRETE

A self-compacting fiber concrete according to the principles developed by Grünewald<sup>4</sup> was developed with the mixture composition shown in Table 1. The mixture had an average 28-days cube compressive strength of  $f_{ccm} = 111.2$  MPa, measured on 12 cubes 150 mm<sup>3</sup> (SD  $s = 5.9$  MPa). Hooked-end steel fibers were used with a

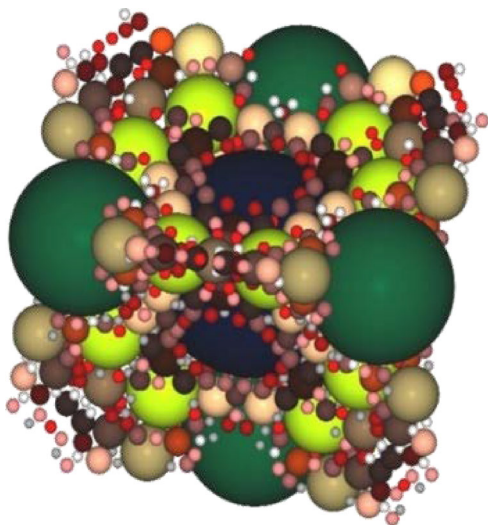


FIGURE 1 Optimizing the packing density (Geisenhandlücke<sup>1</sup>)



FIGURE 2 Reinforcement in a pile cap in traditional reinforced concrete

TABLE 1 Concrete composition

Constituent	kg/m <sup>3</sup>
CEM I 52.5R	566.5
Blast furnace slag	170.0
Silica fume	40.2
BASF Glennium 51	6.2
Water	191.6
Sand 0/4	757.1
Porphyry 2/6	633.5
Steel fibers $l/d = 30/0.38$	61.8
Total	2427

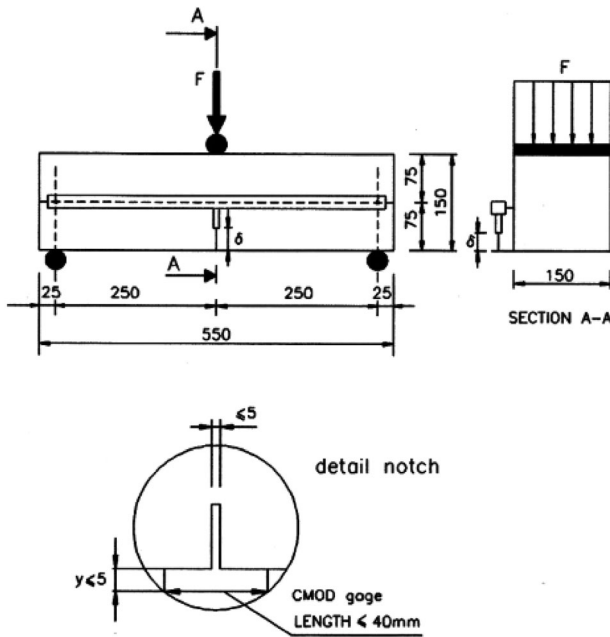


FIGURE 3 Bending test on the notched prism

length of 30 mm and a diameter of 0.38 mm ( $L/d = 79$ ). On the basis of those tests, the concrete strength class was qualified as C80/95. The post-cracking tensile properties of the concrete were determined in a series of 12 notched beam tests.

Figure 3 shows a test specimen with a notch, subjected to three-point bending, according to EN 14651. This method of testing is also suggested by the *fib* Model Code 2010.<sup>2</sup> During the tests, the crack mouth opening displacement (CMOD) at the end of the notch is measured. Figure 4 shows the 12 load–CMOD relations obtained in the three-point bending tests. The relations are used to derive the post-cracking tensile strength properties of the fiber concrete. To that aim the residual flexural tensile strength  $f_{R,j}$  can be calculated for various values of the CMOD with Equation (1)

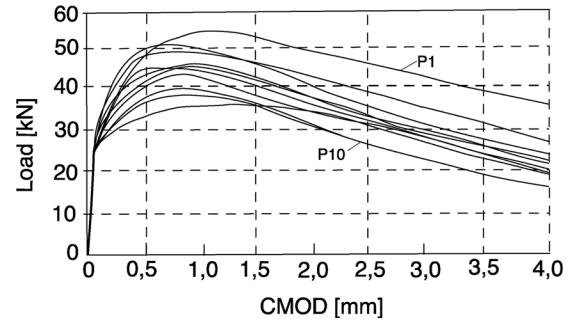


FIGURE 4 Load–CMOD relations for tests on notched beams

$$f_{R,j} = \frac{3F_j l}{2bh_{sp}^2}, \quad (1)$$

where  $F_j$ , (MPa) is the load corresponding to  $CMOD_j = CMOD_j$

$l$ , (mm) is the span length

$b$ , (mm) is the specimen width

$h_{sp}$ , (mm) is the distance between the notch tip and the top of the specimen (125 mm)

The results of the 12 bending tests have been collected in Table 2, for CMOD values of 0.5, 1.5, 2.5, and 3.5 mm. At the bottom of the table the mean values, the standard deviations, and the coefficient of variation for any CMOD are given.

For design purposes, the most important parameters are the values  $f_{R1}$  and  $f_{R3}$  determined for  $CMOD_1 = 0.5$  mm and  $CMOD_3 = 2.5$  mm, respectively.

From those parameters, the tensile strength values in the post-cracking stage relevant for design are derived. For the post-cracking stage, the *fib* Model Code 2010 gives two simplified stress–crack opening relations. These relations are shown in Figures 5 and 6.

For the rigid-plastic relation shown in Figure 5  $f_{Ftu}$  is derived from  $f_{R,3}$  according to the relation:

$$f_{Ftu} = \frac{f_{R,3}}{3}. \quad (2)$$

For the inclined linear relation shown in Figure 6 the parameters  $f_{Fts}$  and  $f_{Ftu}$  follow from:

$$f_{Fts} = 0.45f_{R1}, \quad (3)$$

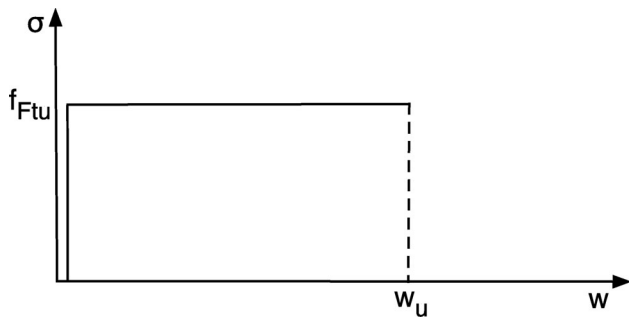
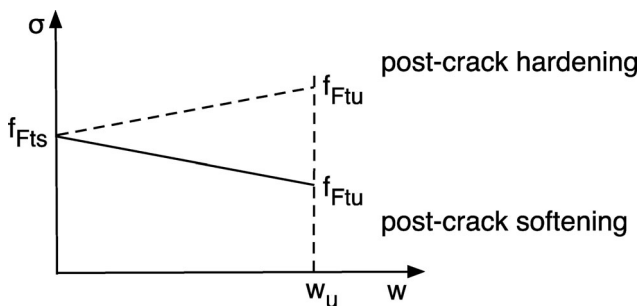
and

$$f_{Ftu} = f_{Fts} - \frac{w_u}{CMOD_3} (f_{Fts} - 0.5f_{R3} + 0.2f_{R1}) \geq 0, \quad (4)$$

where  $w_u$  is the maximum crack width accepted in structural design for the case considered. In general  $w_u = 1.5$  mm is assumed.

TABLE 2 Limit of proportionality (LOP) and post-cracking tensile strengths  $f_{Ri}$ 

Specimen	LOP (MPa)	$f_{R,1}$ (MPa) for CMOD <sub>1</sub> = 0.5 mm	$f_{R,2}$ (MPa) for CMOD <sub>2</sub> = 1.5 mm	$f_{R,3}$ (MPa) for CMOD <sub>3</sub> = 2.5 mm	$f_{R,4}$ (MPa) for CMOD <sub>4</sub> = 3.5 mm
P-1	7.7	14.9	17.3	14.4	12.5
P-2	8.0	13.4	13.0	11.6	9.7
P-3	7.0	14.0	13.7	12.5	10.1
P-4	7.4	10.6	11.7	10.5	8.8
P-5	8.3	11.9	12.8	11.1	9.2
P-6	7.5	11.7	11.6	10.2	8.1
P-7	8.7	15.5	14.9	11.2	8.6
P-8	9.6	15.7	15.4	12.4	9.6
P-9	8.8	14.4	12.7	10.6	9.0
P-10	8.4	13.2	11.7	8.2	6.0
P-11	8.4	13.4	11.8	9.7	7.5
P-12	9.4	14.8	12.7	10.1	8.1
Mean value $x_m$	8.34	13.6	13.35	11.02	8.93
SD	0.70	1.58	1.77	1.57	1.58
COV (%)	8.3%	11.6%	13.6%	14.5%	17.7%

FIGURE 5 Rigid plastic relation between stress  $\sigma$  and crack opening  $w$  (fib MC 2010<sup>2</sup>)FIGURE 6 Linear relation between post-cracking tensile stress  $\sigma$  and crack opening  $w$  (fib MC 2010<sup>2</sup>)

An overview of the relevant post-cracking tensile stresses is given in Table 3. In this table also the mean and characteristic tensile strength values of the concrete

$f_{ctm}$  and  $f_{ctk}$  are given, which also form part of some design equations.

Looking at the results of the tests, given in Tables 2 and 3, a number of conclusions can be drawn. From Table 2 it follows that the scatter of the notched beam test is remarkably small. For 12 tests the coefficient of variation of the parameter  $f_{R,1}$  is  $CoV = s/f_{Rm,1} = 1.59/13.63 = 11.6\%$ . For the parameter  $f_{R,3}$  the coefficient of variation is  $CoV = s/f_{Rm,3} = 1.57/11.02 = 14.2\%$ . In general the notched beam tests according to Figure 3 are known to give a substantial scatter, with a CoV of more than 20%, because of the small dimensions of the cross-section above the notch, governing the load–CMOD relation. The results of the notched beams tests carried out in this program indicate a homogeneous mixture, with low sensitivity to irregular fiber orientation and distribution. In a subsequent part 2 of this paper, the fiber orientation and distribution, as measured in the various test specimens will be dealt with more in detail.

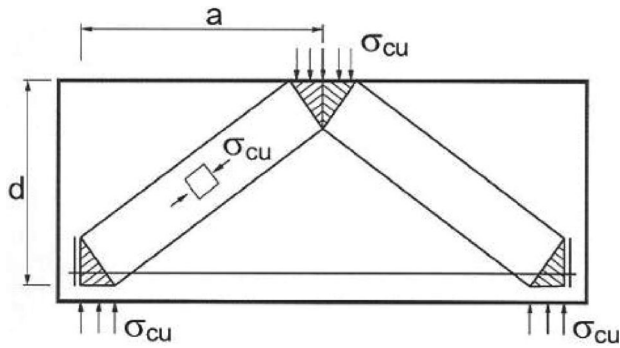
A second, important observation from Table 3 is the relatively high value of the mean axial post-cracking tensile strength, immediately upon cracking, which is  $f_{Ftsm} = 6.1$  MPa. For a concrete strength class C80/95 the mean tensile uniaxial cracking strength of the concrete is  $f_{ctm} = 4.8$  MPa. This means that after crack formation in a structural member the cracks will not widen, but instead, new cracks will occur at increasing deformation. This means that many cracks with very small widths will occur instead of single wider cracks. This has not only a positive effect on durability but can also mean a



**TABLE 3** Tensile strength values in the post-cracking stage relevant for design

Symbol	Denotation	Derived from test values according to	Value (MPa)	Relevant for
$f_{Ftum}$	Mean axial post-cracking tensile strength	$f_{Ftum} = f_{R3,m}/3$	3.7	General analysis of behavior, bending capacity
$f_{Ftuk}$	Characteristic post-cracking axial tensile strength	$f_{Ftuk} = f_{R3,k}/3$	2.8 <sup>a</sup>	Used in combination with rigid-plastic relation, bending. For punching shear in the absence of longitudinal reinforcement
$f_{Ftsm}$	Mean axial post-cracking tensile strength at small crack width	$f_{Ftsm} = 0.45 f_{R1,m}$	6.1	Crack width control
$f_{Ftsk}$	Characteristic post-cracking tensile strength at small crack width	$f_{Ftsk} = 0.45 f_{R1,k}$	4.9	Check of tensile stress in SLS ( <i>fib</i> MC 2010), Ch. 7.7.4.1
$f_{ctm}$	Mean tensile strength of concrete	Strength class C80/95	4.8	Crack width control
$f_{ctk}$	Characteristic tensile strength of concrete	Strength class C80/90	3.4	Shear resistance

<sup>a</sup>The *fib* Model Code 2010 allows in certain cases as well a determination of  $f_{Ftuk}$  using Equations (3) and (4). In this case, the value  $w_u$  should be known. For shear and punching shear (fiber concrete in combination with longitudinal reinforcement) the value  $w_u = 1.5$  mm is suggested. In combination with the values for  $f_{Ftsm}$ ,  $f_{R1,m}$ , and  $f_{Rm,3}$  this would lead to  $f_{Ftuk} = 3.15$  MPa.

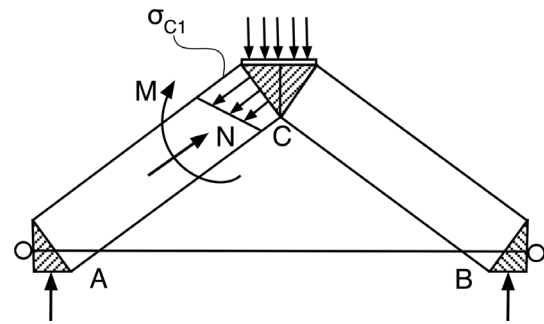
**FIGURE 7** Regular strut-and-tie model for short beam

significant increase of the shear bearing capacity, because a bundle of cracks with small widths is able to transmit substantially larger shear friction stresses by virtue of aggregate interlock than single wider cracks.

### 3 | EXPERIMENTS ON STRUCTURAL MEMBERS

#### 3.1 | Shear tests on short deep beams

For pile caps, strut-and-tie models are an excellent design tool. In Figure 7 the basic idea of designing a short reinforced concrete beam without shear reinforcement using a strut-and-tie model is shown. This idealized 2-D representation suggests that the compression struts have a prismatic shape and that they fail by concrete crushing. However, as demonstrated by tests on short beams carried out by Walraven/Lehwalter<sup>5</sup> this is a considerable simplification of the real behavior. From their experiments, it was

**FIGURE 8** Strut-and-tie model with two hinges (points A and B) and a fixed node (point C), according to Walraven/Lehwalter<sup>5</sup>

found that the shear capacity of the beams does not only depend on the concrete strength and the size of the strut (related to the area of the load introduction) but as well on the flexural reinforcement ratio and the ratio  $a/d$  of the beams. Moreover, a size effect was observed and it was concluded that the axial compressive strength in the strut is not the most suitable failure criterion if more accuracy is strived after: an analysis showed that the accuracy of the strut-and-tie model can be improved by assuming a fixed node at the top (Fig. 8) and using the stress  $\sigma_{c1}$  in the upper part of the strut, which is a function of the normal force  $N$  and the bending moment  $M$  (due to deformation of the longitudinal tie at the bottom), as a limit criterion.

The size effect can be explained by assuming a localized failure zone at the junction between the strut and the upper node. This model confirms the role of the parameters concrete strength, longitudinal reinforcement, size, and slenderness, which are also involved in the basic expression for the shear resistance of concrete

members without shear reinforcement found in the Eurocode for Concrete Structures EN-1992-1-1. For the determination of the shear resistance of short beams with a load near to the support the following expression will be used, which is an extension of the corresponding equation in EN-1992-1-1, Chapter 6.2.2 Equation 6.2.a

$$V_{Rd,c} = \eta C_{Rd,c} \kappa (100 \rho_l f_{ck})^{\frac{1}{3}} b_w d, \quad (5)$$

where  $f_{ck}$  is the characteristic cylinder compressive strength in MPa,  $k$  is the size factor defined as  $k = 1 + \sqrt{200/d} \leq 2.0$  with  $d$  in mm,  $\rho_l$  is the longitudinal reinforcement ratio  $\frac{A_{sl}}{b_w d} \leq 0.02$ , and  $C_{Rd,c}$  is a parameter based on an evaluation of test results, the final value of which can be chosen by the countries, with a default value of 0.12. The factor  $\eta$  is a magnification factor for shear resistance of beams with loads near to supports, which depends on the ratio  $a_v/d$ , where  $a_v$  is the horizontal distance between the inner edge of the support and the edge of the load introduction area at the upper side of the beam. In EN 1992-1-1 Ch. 6.2.2(6), the effect of a concentrated load near to the support is accounted for by the factor  $\beta = a_v/2d$ , where  $\beta$  is used as a reduction factor for the load. Here  $\eta$  is used as a magnification factor for the shear resistance, so basically  $\eta = 1/\beta$ . So, following EN 1992-1-1  $\eta$  should be  $\eta = 2d/a_v$ . Compared with tests on reinforced short beams with a load near to the support this expression turns out to be rather conservative (Regan,<sup>6</sup> Walraven<sup>7</sup>). A point of consideration is the mechanism of load transmission from load to support. In short deep beams during loading, an inclined shear crack develops which propagates through the strut from the edge of the support to the edge of the loaded area. This crack formation weakens the strut capacity. The degree of strength reduction depends on the shape of the inclined shear crack. The high-performance fiber concrete mixture developed in this project has a post-cracking tensile strength which is higher than the cracking tensile strength of the concrete (compare the cracking and post-cracking tensile strengths  $f_{ctm} = 4.8$  MPa and  $f_{tsm} = 6.1$  MPa in Table 3). That implies that the damaging effect of the inclined cracks on the strut capacity is reduced in comparison with concrete without steel fibers, especially when they create a hardening effect. This explains why the factor  $\beta$  in Equation (5) can be increased beyond the value  $\beta = 2d/a_v$  as used in EN 1992-1-1 for concrete without fibers.

Equation (5) was extended to make it applicable for fiber reinforced concrete in the *fib* Model Code 2010, Chapter 7.7.3.2.2. The modified equation is

$$V_{Rd,c} = \eta C_{Rd,c} \kappa \left[ 100 \rho_l \left( 1 + 7.5 \frac{f_{Ftuk}}{f_{ctk}} \right) \right]^{\frac{1}{3}} b_w d, \quad (6)$$

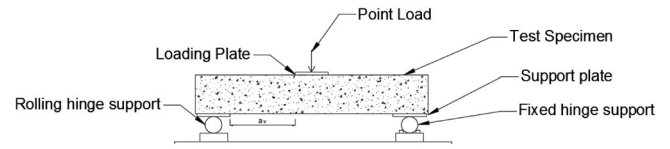


FIGURE 9 Experimental set-up for shear tests on short HPFC reinforced beams

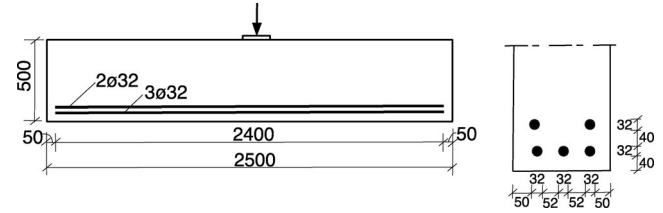


FIGURE 10 Reinforcement scheme beam series 1

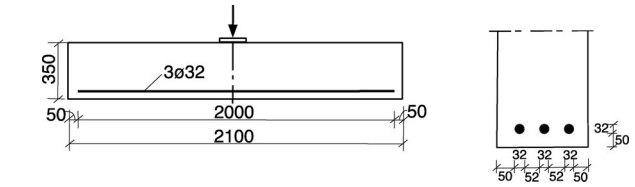


FIGURE 11 Reinforcement scheme beam series 2

where  $f_{Ftuk}$  is the characteristic value of the ultimate post-cracking tensile strength for fiber reinforced concrete (see also Table 3 in this paper); furthermore,  $f_{ctk}$  is the characteristic tensile strength of the concrete matrix.

To verify the suitability of Equation (6) for the HPFC mixture used in this investigation two series of shear tests on short beams with a load near to the support were carried out. The test set-up is shown in Figure 9. The support areas had a size of 150 mm × 300 mm × 25 mm. The dimension of the loading plate was 150 mm × 300 mm × 25 mm.

In total 6 three-point shear tests on short beams loaded by a concentrated load at midspan were carried out, which can be subdivided into two series of 3 beams each. The beams in the first series had a cross-sectional height of 500 mm and a width of 300 mm and were reinforced with 5 rebars with a diameter of 32 mm (Figure 10). The beams of the second series had a cross-sectional height of 350 mm and a width of 300 mm and contained 3 rebars with a diameter of 32 mm (Figure 11). The reinforcement ratios of the beams in series 1 and 2 were 3.20% and 2.83%, respectively. Those relatively high reinforcement ratios were chosen to make sure that all elements would fail in shear.

In each series three different specimens were tested, where the ratio  $a_v/d$  varied between 2.0, 1.5, and 1.0 (the

load was always introduced at midspan but between the tests, the supports were symmetrically shifted into the direction of mid-span, to vary  $a_v/d$ . During the tests, all beams were subjected to a displacement-controlled load for which the displacement at mid-span of the beam was increased at a rate of 0.010 mm/s until the maximum capacity of the beam was attained. Subsequently, the displacement rate was increased up to a maximum of 0.2 mm/s to obtain a well-controlled post-peak behavior. Next to monitoring the vertical displacement at mid-span and the applied load, also electrical strain gauges were placed at one side of each beam to monitor the development of shear and flexural cracks during loading (Figure 12). Furthermore, visual inspections of the crack pattern were carried out after each load increment of 150 kN. As expected, all beams

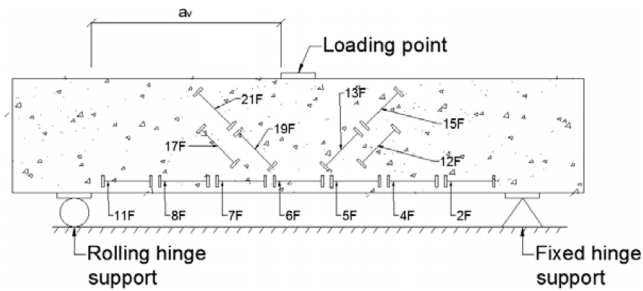


FIGURE 12 Schematization of test set-up for the HPFC beams



FIGURE 13 Beam B-6 after shear failure

failed in shear-flexure as shown in Figure 13. At the end of the inclined shear crack, in all tests local failure of the compression zone adjacent to the load application point was observed (Droogné/De Ghein<sup>8</sup>).

To compare the results of the shear tests with the theoretical predictions the design Equation (6) was modified in the following way: at first, to get the mean values of the shear resistance, the coefficient  $C_{Rd,c}$  was replaced by the value  $C_{Rm,c} = 0.19$  (for the relation between the value  $C_{Rd,c}$  used in EN 1992-1-1 and the average value  $C_{Rm,c}$  reference is made to<sup>9,10</sup>). Secondly, the mean concrete strength  $f_{cm}$  was used instead of the characteristic strength  $f_{ck}$ . Thirdly the conservative value  $\eta = 2d/a_v$  according to EN 1992-1-1, was replaced by  $\eta = 3.5d/a_v$  which gives the best agreement with the test results. Next, the limitation of the upper value of the longitudinal reinforcement, which in EN 1992-1-1 is limited to an upper value of 2%, has been omitted. Applying those assumptions good agreement is obtained between the experimental shear resistance  $V_{u,exp}$  and the theoretical values  $V_{u,th}$  obtained with Equation (6) modified to predict mean values, see Figure 14 and Table 4. The large post-cracking tensile strength of the HPFC plays a positive role. Concerning the magnification factor  $\eta$  no sensitivity for the

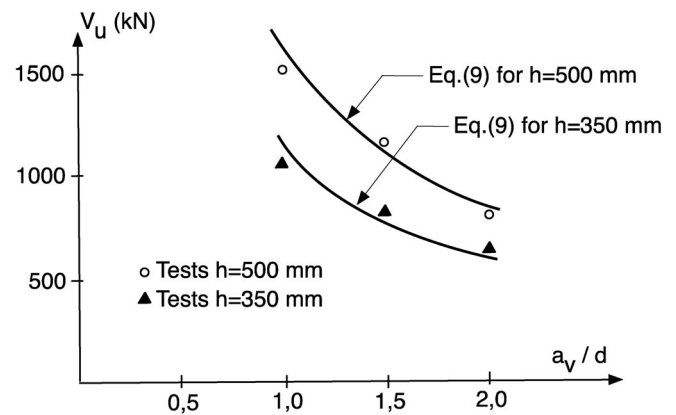


FIGURE 14 Comparison between experimental shear resistance and theoretical values

TABLE 4 Summary results of the tests on short HPFRC beams

Beam number	Height (mm)	Effective depth (mm)	Longitudinal reinforcement ratio (%)	$a_v/d$ (—)	$P_{exp,max}$ (kN)	$V_{u,exp}$ (kN)	$V_{u,th}$ [kN]	$V_{u,exp}/V_{u,th}$ [—]
B-1	500	415.2	3.20	2.0	1522.1	806.6	844	0.96
B-2	500	415.2	3.20	1.5	2270.8	1189.9	1124	1.06
B-3	500	415.2	3.20	1.0	2949.3	1520.2	1687	0.90
B-4	350	284	2.83	2.0	1172.3	624.4	599	1.04
B-5	350	284	2.83	1.5	1531.0	803.7	797	1.01
B-6	350	284	2.83	1.0	2092.0	1084.2	1177	0.92



cracking pattern needs to be expected, because the post-cracking tensile stress, transmitted by the fibers across the crack, is higher than the cracking strength of the concrete. Therefore, a magnification factor of  $\eta = 3.5d/a_v$  appears to be a realistic value for predicting the mean value of the shear resistance. The relative insensitivity of the fiber concrete to crack formation of any type should allow as well an increase of the upper limit of the longitudinal reinforcement ratio in Equation (6).

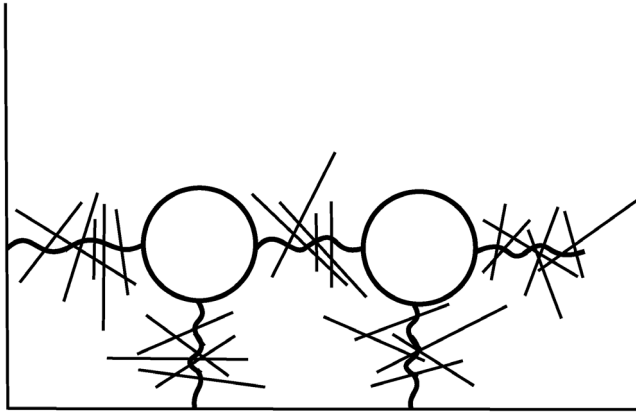
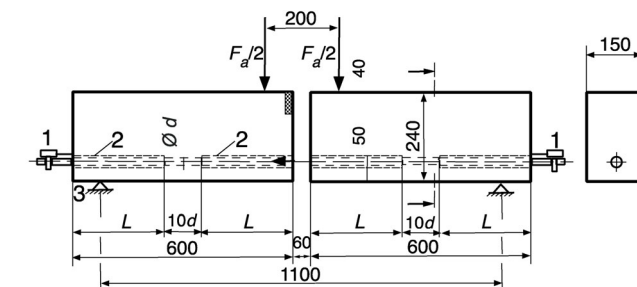


FIGURE 15 Confining effect of steel fibers on required anchorage length



Key  
1 slip measuring device  
2 plastic sleeves  
3 movable support

FIGURE 16 Experimental set-up for bond test according to RILEM,<sup>11</sup> EN 10080:2005

### 3.2 | Bond and anchorage of reinforcing bars in HPFC

For the anchorage length of reinforcing bars in plain concrete expressions are found in codes that consider a dependency on a number of influencing parameters, like bar diameter, the thickness of the cover, and confinement. However, confinement is only related to the effect of reinforcing bars in the transverse direction, like stirrups. In a similar way from fibers a confining effect on the bond and the required anchorage length may be expected, Figure 15.

To determine the confining effect of the fibers a series of experiments have been carried out on the anchorage capacity of reinforcing bars in HPFC used in this research program. The experimental set-up corresponded with the test method developed by RILEM,<sup>11</sup> see Figure 16.

The beam, which is equipped with a steel hinge in the compression zone at mid-span, so that the inner lever arm is accurately known, is subjected to 4-point loading: in this way, the tensile force in the reinforcement can be determined accurately. According to the standardized procedure, the reinforcing bar is placed in a plastic sleeve, which leaves a length of  $l_b = 10\phi$  along which the bar is bonded to the concrete. In the actual test series, the bonded length is used as a variable with values ranging from 6 to  $12\phi$ . In the test series, the bar diameter was always 25 mm. The slip of the bar during loading was measured at the end of the beam. In this way bond-slip relations are obtained. If the pull-out force in one of the beam halves was reached, that part was clamped, so that also the other half of the beam could be loaded until the maximum pull-out force was reached. So, for every beam two test results were obtained. The test series consisted altogether of 8 experiments. Four beams have been made of plain concrete (the BS-series) and 4 beams of fiber concrete (the B-series). An overview of the tests is given in Table 5.

The tests showed that the behavior of the two sides did not differ very much so that the reproducibility appeared to be good. In Figure 17, the pull-out load versus slip relations are shown for the beams B-2 and BS-2 (with  $l_b/\phi = 8$ ). In Figure 18, the corresponding curves

TABLE 5 Comparison between pull-out forces for beams with and without fibers

Specimen nr.	Ratio $l_b/\phi$	Max. pull-out force with fibers (mean value, kN)	Max. pull-out force without fibers (mean value, kN)	Ratio pull-out force with/without fibers
B-1 and BS-1	6	168.7	145.2	1.16
B-2 and BS-2	8	197.5	141.3	1.40
B-3 and BS-3	10	237.8	161.2	1.48
B-4 and BS-4	12	232.3	170.3	1.36

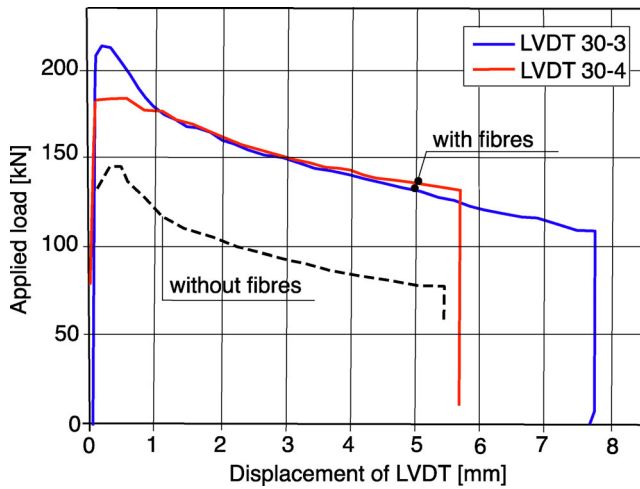


**FIGURE 17** Pull-out load-slip relations for beams B-2 and BS-2 ( $l_b/\phi = 8$ ) showing the difference between fiber concrete beam (B-2; red and blue solid lines) with the corresponding plain concrete beam (BS-2: dotted line)

are shown for the beams B3 and BS3 (with  $l_b/\phi = 10$ ). It turns out that the fibers lead to an approximately constant enhancement of the pull-out force over the whole range of displacement. This expresses the effect of the fibers on reducing crack propagation and opening. Table 5 shows that the smallest increase of the anchorage capacity is obtained for the smallest ratio  $l_b/\phi = 6$  (increase with factor 1.16). For larger values of  $l_b/\phi$  the increase of the anchorage capacity is in the range 1.36–1.48. Real anchorage lengths in engineering practice are considerably larger than tested here (values of  $l_b/\phi < 30$  are seldom). Therefore, it seems reasonable to assume that the increasing factor of the pull-out load by the effect of fibers is at least 1.25, which would lead to a safe reduction of the anchorage length to 80% of the length in plain concrete.

### 3.3 | Bearing capacity of pile caps in HPFC supported by piles

A series of 4 experiments were carried out on solid slab foundation elements supported by piles (Droogné, De Ghein<sup>12</sup>). The experiments were carried out to study the effect of fibers on the bearing capacity and to develop a design method for such structural elements. The dimensions of the slabs are shown in Figure 19. The specimen P-1 was chosen as a reference specimen. It was reinforced with ties between the supports, each consisting of 3 reinforcing bars  $\phi$  25 mm. The specimens P-3 and P-4 had identical ties but additionally contained 60 kg/m<sup>3</sup> fibers. The specimen P-2, contained only fibers, but no reinforcing bars. The results are given in Table 6.

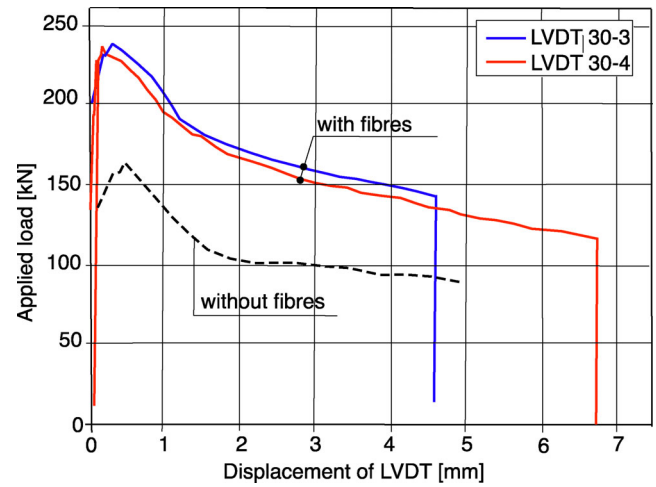


**FIGURE 18** Pull-out load-slip relations for beams B-3 and BS-3 ( $l_b/\phi = 10$ ) showing the difference between fiber concrete beams (B-3; red and blue solid lines) with the corresponding plain concrete beam (BS-3: dotted line)

Figure 20 shows the relations between the central load and the central deflection measured in the test.

The curves for the specimens P-3 and P-4, which are similar, show a good agreement with each other. Moreover, they show ductile behavior. The curve P-1 (only reinforcement, no fibers) reaches its maximum value at about the same central deflection as P-3 and P-4 but reacts in a less ductile way after passing the top. It is seen that the addition of 60 kg/m<sup>3</sup> fibers increases the capacity by about 65%. The slab with only fibers (P2) reaches its maximum at a smaller deflection than the other slabs. This is due to the way of testing. A displacement-controlled test on specimens with such large dimensions is hardly possible. There is a substantial amount of energy stored in the loading frame when reaching the maximum load level during the test. After passing the top this energy is released, and the test is rather load-controlled than displacement-controlled, which goes along with a steep descending branch. In the slabs with a combination of fibers and tensile ties between the supports (P3 and P4), the release of energy will not occur that abruptly, because a “second bearing mode” by the strut-and-tie mechanism allows a further increase of the load. In that case, the contribution of the fibers will be better stabilized after passing the top than is the case in test P2 (that would mean an approximately constant contribution of the fibers to the total bearing capacity instead of the descending branch for specimen P2 after a deflection of 5.0 mm. This is confirmed by the results of the tests, where the maximum bearing capacity of the specimen with only reinforcing ties (P1) is 1735 kN, and the maximum bearing capacity of the specimen with only fibers (P-2) is 1035 kN. The sum of the two is 1735

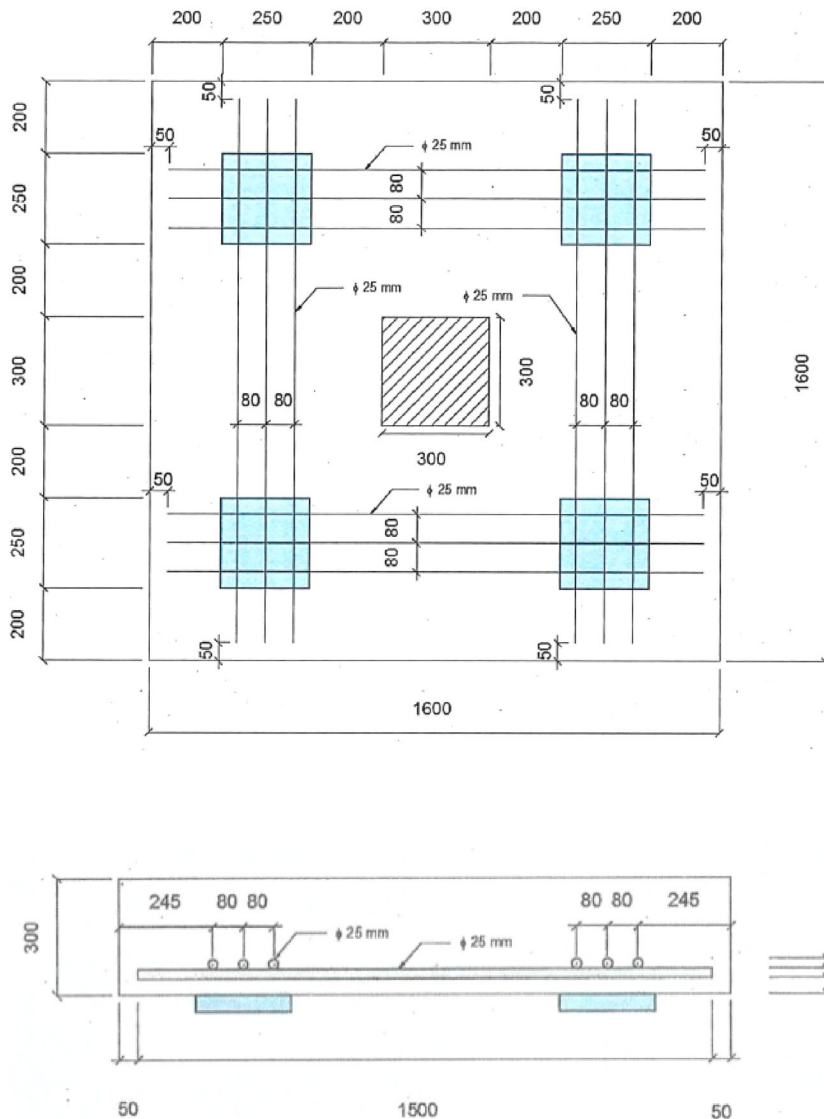


FIGURE 19 Specimen dimensions for tests on slabs supported by piles

TABLE 6 Overview of tests on solid slabs

Slab designation	Ordinary reinforcement	Steel fibers	Maximum load (kN)	Maximum deflection (mm)
Slab P-1	Yes	No	1735.35	14.17
Slab P-2	No	Yes	1035.44	39.42
Slab P-3	Yes	Yes	3014.08	16.78
Slab P-4	Yes	Yes	2826.23	24.22

+ 1035 = 2770 kN, which is not far below the bearing capacity of the specimens with both reinforcing steel and fibers, which resisted loads of 2826 kN and 3014 kN respectively.

Visual control of the specimens P-3 and P-4 after failure shows a yield line pattern that develops from the center of the slab to the corners and to the edges (Figure 21).

The diagonal cracks seen at the bottom of the slabs are required to activate the strut and tie mechanism. After the maximum capacity of those “diagonal yield lines” has been exhausted because of slip of the fibers, the strut-and-tie model has to carry the additional load, which ends when one of the components of the strut and tie mechanism has reached its capacity (struts or nodes between struts and reinforcing ties). The slab P-1 with

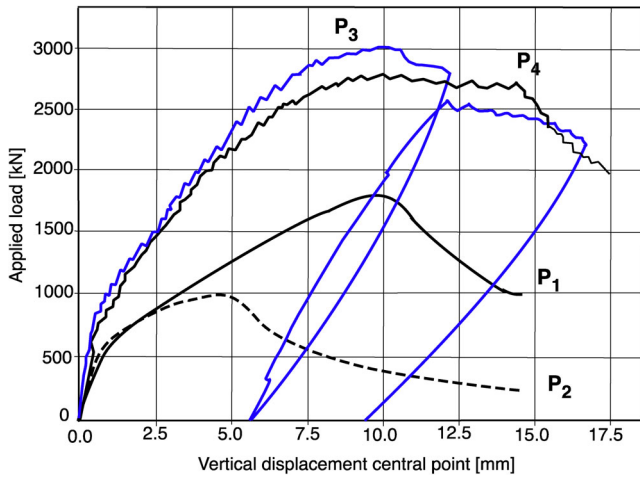


FIGURE 20 Load-deflection relations for the foundation slabs



FIGURE 21 Crack pattern at bottom of slab P-3 (with fibers and ties) after the test

only fibers failed in bending, by a single bending crack (Figure 22).

The behavior of the slabs with fibers and ties can be represented in a simplified way. Figure 23 shows a 3-D strut-and-tie system to carry the load. It was argued earlier that a strut-and-tie system does not take account of the effect of  $a_v/d$ , nor a size effect, on the bearing capacity. As an alternative for a strut and tie system, the behavior can be represented by a system of two short beams following the diagonals of the rectangular slab, Figure 24. This two-beam system is used for further evaluation. The mean capacity of the (individual) short deep beams can be determined with Equation (6) replacing  $C_{R,c}$  by  $C_{R,d}$ ,  $m = 0.19$  and  $f_{ck}$  by  $f_{cm}$ :

In Equation (6), for the system of diagonal short beams (Figures 24 and 25) the “equivalent” reinforcing ratio  $\rho_L$  of the beams in the diagonal directions, has to be calculated on the basis of the reinforcing ties in the bottom of the element, between the supports in the corners

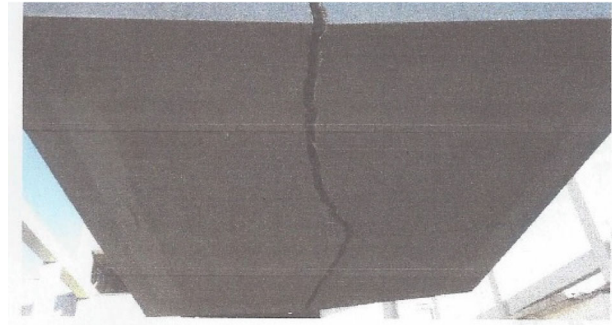


FIGURE 22 Failure pattern of fiber concrete slab without ties (P-1)

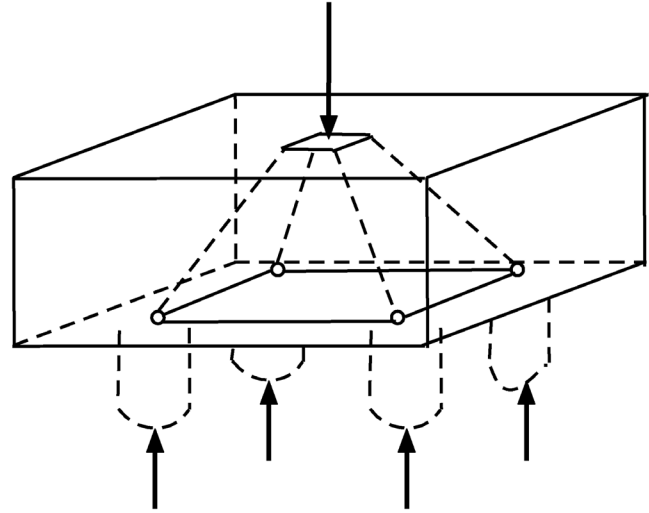


FIGURE 23 Strut and tie system

(see also Figure 19). From Figure 25 (top view on slab specimen) the dimensions of the short beams, and the equivalent diagonal reinforcement ratio  $\rho_{Leq}$ , can be derived. For ease of use, the supports and the load introduction areas have been turned over  $45^\circ$ . It is assumed that the ties, meeting each other at support, can be composed of a fictitious reinforcement in the diagonal direction. In Figure 19, it is shown that any tie consists of 3 bars  $\phi 25$  which corresponds with  $A_s = 1470 \text{ mm}^2$ . The cross-sectional area of the fictitious reinforcement in the diagonal direction is then  $1470 \cdot \sqrt{2} = 2079 \text{ mm}^2$ . With an average width of the diagonal beam of 275 mm and an effective height of 235 mm, the “fictitious” reinforcing ratio in the diagonal direction is  $\rho_1 = 2079 / (275 \cdot 235) = 3.2\%$ . From the mixture properties (Table 3) it follows that  $f_{Ftum} = f_{R3,m}/3 = 11.02/3 = 3.7 \text{ MPa}$ . Moreover  $f_{ctm} = 4.8 \text{ MPa}$ . The size factor is  $k = 1 + (200/d)^{0.5}$ . With  $d = 235 \text{ mm}$  it is found that  $k = 1.92$ . The magnification factor  $\eta = 3.5(235/397) = 2.07$ . Finally,  $f_{cm}$  (mean concrete cylinder compressive strength) is assumed to be

$f_{ck} + 8 = 88$  MPa. Implementing those parameter values into the modified Equation (6) results in  $V_{Rcm} = 604$  kN at both sides of the diagonal beam. So, the bearing capacity of one diagonal beam is  $2V_{Rcm} = 1208$  and the

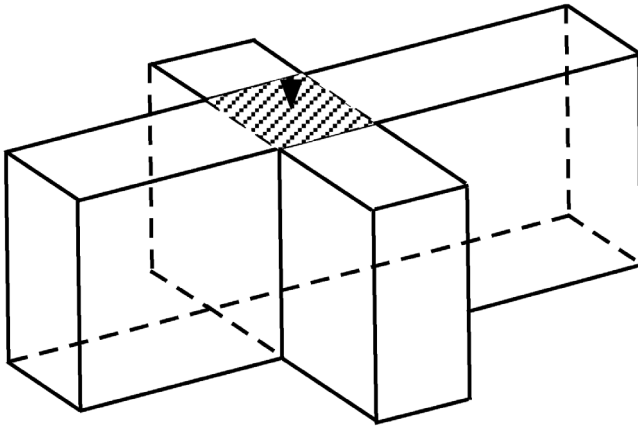


FIGURE 24 System with two diagonal short deep beams

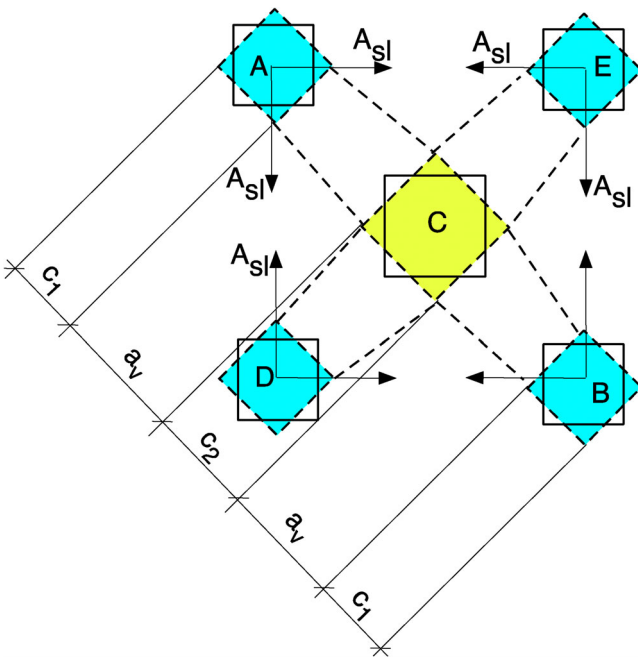


FIGURE 25 Top view on foundation element with simplification to double short beam system

bearing capacity of the slab (based on the two diagonal beams) is  $P_u = 2 \cdot 1208 = 2416$  kN (Table 7). This is lower than the bearing capacity of the slabs measured in the experiments, where for specimen P-3 a value 3014 kN was found and for P-4 a value 2826 kN. However, it should be noted that ignoring the role of fibers in the stiffness of the tensile ties is a conservative assumption. Moreover, the effective width of the diagonal beams will be larger than the width of the prismatic struts as assumed. Taking those aspects into account an improvement of the agreement between model and experiments could be obtained. This is not further pursued here, because those tests intended to propose a simple model, reliable, and accurate enough for practical design.

Slab P-1 was, with regard to its geometry, similar to the specimens P-3 and P-4, but did not contain fibers. Assuming  $f_{Ftum} = 0$  in the modified Equation (6) eliminates the effect of fibers and leads to a predicted bearing capacity of this slab equal to 1277 kN, whereas the experimental resistance was measured to be 1735 kN. So in this case the simplified model used leads to a conservative estimation of the bearing capacity. One reason for this conservatism is the assumed independence of the two diagonal beams, the bearing capacity of which is just added. In reality there is an interaction. In a single short deep beam failure is mostly initiated in the load introduction zone at the top of the specimen. In the case of combined beams, the load introduction area is confined as a result of the interaction between the two beams (3-D compression), which increases the bearing capacity. In beams with fibers this effect is further enhanced by the confining action of the fibers.

Finally, slab P-2, with only fibers but no tensile ties consisting of reinforcing bars, still carried a relatively large load of 1035 kN. Assuming a rigid-plastic post-cracking behavior (Figure 5) with a tensile strength of  $f_{Ftum}$ , and an estimated height of the compression zone of  $0.1 h$ , the ultimate bending moment is equal to:

$$M_u = 0.45bh^2f_{Ftum}. \quad (7)$$

Substituting  $h = 300$  mm,  $b = 1600$  mm, and  $f_{Ftum} = 3.7$  MPa (Table 3) it is found that  $M_u = 240$  kNm.

TABLE 7 Comparison between experimental bearing capacity and bearing capacity determined with simplified models

Slab number	Ordinary reinforcement	Steel fibers	Maximum load in test (kN)	Maximum load determined with a simple (conservative) model (kN)
Slab P-1	Yes	No	1735	1277
Slab P-2	No	Yes	1035	1010
Slab P-3	Yes	Yes	3014	2416
Slab P-4	Yes	Yes	2826	2416



For the failure pattern shown in Figure 22, with a single governing crack, the ultimate load is  $P_u = 4M_u/l = 4 \cdot M_u / 0.95 = 1010$  kN. This corresponds well with the value of 1035 kN found in the experiment.

#### 4 | APPLICABILITY OF HIGH PERFORMANCE FIBER CONCRETE IN THE INTERMEDIATE STRENGTH RANGE IN GENERAL

Classification of fiber concrete in conventional strength classes, as practiced in design recommendations, only gives a limited indication for applicability. In conventional structural concrete, according to governing building codes, nearly all properties, both in a mechanical and a physical sense, improve with the increasing strength of the concrete. So all properties are related to the concrete compressive strength. Contrary to this, in fiber reinforced concrete the properties in the post-cracking stage make the difference. The higher is the post-cracking tensile strength of a fiber reinforced concrete in comparison with the tensile strength of the concrete at cracking, the more favorable the behavior will be, both in the serviceability limit state and in the ultimate limit state. In the serviceability limit state the crack width will be small, which is beneficial for durability. In the ultimate limit state fine cracks, especially in shear-loaded structures, can increase the bearing resistance, as a result of the increased aggregate interlock contribution in the cracks. If the concrete mixture is composed in such a way that the post-cracking tensile strength is higher than the tensile strength of the concrete without fibers, cracks will hardly open after formation, because the cracking strength is smaller than the stress necessary to open the cracks. This results in multiple cracking, which is a favorable property for instance for coping with imposed deformations. Such properties are known from special concretes like engineered cementitious composites (Li<sup>13</sup>), in which the tensile strength of the concrete was kept artificially low to realize multiple cracking behavior. However, it was shown in this research program that such a behavior can also be realized with fiber concrete in the higher strength ranges so that the advantage of the multiple cracking behavior goes along with the advantages obtained by a higher strength.

An aspect to be regarded as well is the sensitivity of a concrete to fiber orientation. In the most actual design concepts, like [fib MC 2010] and the draft version of the Eurocode 1992-1-1, with Annex L devoted to fiber concrete, the effect of fiber orientation can be compensated by the ability of a structure to internally redistribute its forces. However, if a fiber concrete can be shown to be less

sensitive to fiber orientation, less value has to be imposed on the redistribution capacity of the structure. For concrete that is less sensitive to the occurrence of fiber orientation, also the other properties as determined in experiments are more reliable. In this respect, the low scatter in the experiments gives good confidence. More than traditional concrete fiber reinforced concrete can be designed for properties. In this research program, it was shown that favorable properties with regard to strength, stiffness, ductility, durability, and workability can be combined in one single “high performance” fiber concrete.

#### 5 | APPLICABILITY OF A HIGH-PERFORMANCE FIBER CONCRETE IN THE INTERMEDIATE STRENGTH RANGE FOR THE DESIGN OF FOUNDATIONS

The research carried out in his program was inspired by the question of whether a high-performance fiber reinforced concrete could be a good solution for the design of pile caps. Therefore, tests have been carried out on aspects that play a role in the design of pile caps, and short beams. The results showed that the fiber concrete developed in the scope of this program offers many properties which are favorable for the design of foundation elements. Further studies on the design of foundation elements, making use of the properties found in the experiments, showed that the dimensions of such structural elements can be significantly reduced (to about 60%). Furthermore, the volume of reinforcement by reinforcing bars can significantly be reduced. It is often sufficient to design for bending (like using a reinforcing mesh at the bottom for a foundation block like shown in Figure 2), extended with rebars between the supports. The fibers take over all other functions, like shear reinforcement, punching reinforcement, transverse reinforcement in anchorage regions, and various types of minimum reinforcement.

For the design, use can be made of an integral approach to the design of fiber concrete, as found in the fib Model Code for Concrete Structures 2010. Here, the following basic rules can be used:

- The structure is designed for bending in the traditional way with reinforcing steel. The fibers are not taken into account for this aspect of the design.
- For the design in shear, for members without shear reinforcement Equation (6) in this paper can be used, with a magnification factor  $\eta = 3d/a_v$ . This is an extension of Equation (7.4-5) in the fib Model Code 2010.

- For the anchorage length of reinforcing bars a reduction factor of 0.8 can be used, as a result of the confinement of the rebars by the fibers in the anchorage zone (this holds true for the mixture considered).
- All other rules for fiber concrete as given in the *fib* Model Code 2010, see Chapters 5.6 “Fibers/fiber reinforced concrete” (7 pages) and 7.7 “Verification of safety and serviceability of FRC structures” (8 pages) can be used, and are sufficient, for a rational design.

## 6 | CONCLUSIONS

1. There is a lot of experimental evidence and practical experience on both fiber concrete with low/medium strength and with ultra-high-strength concrete. The region in-between, however, offers as well very interesting opportunities, like foundation elements as treated in this paper.
2. Subdividing fiber concretes in strength classes is a practical way to allow fibers to be combined with conventional types of reinforcement. The most important properties of fiber concrete are, however, not related to the concrete compressive strength but to the post-cracking behavior and should be determined separately. This allows taking advantage of the properties of special, defined performance, fiber concrete mixtures.

Defined performance concretes can be designed to combine favorable properties like strength, stiffness, ductility, durability, and workability in one single mixture.

3. The design rules offered in the *fib* Model Code 2010 for fiber reinforced concrete (altogether 15 pages) offer a good basis also for the application of specially designed high-performance fiber concretes. Slight extensions, based on tests, could further widen the applicability of those rules.

## DATA AVAILABILITY STATEMENT

The data that support the findings of this study are available from the corresponding author upon reasonable request.

## ORCID

Joost Walraven  <https://orcid.org/0000-0003-3243-8878>

## REFERENCES

1. Geisenhanslüke C, Influence of the granulometry of fine particles on the rheology of pastes, PhD-thesis, University of Kassel, Structural Materials & Engineering Series, No. 13, Kassel University Press GmbH, Kassel; 2008 (in German).
2. *fib* Model Code for Concrete Structures 2010.
3. Di Prisco M, Colombo M, Dozio D. Fibre-reinforced concrete in *fib* model code 2010: principles, models and test validation. *Struct Concr*. 2013;14(4):342–61.
4. Grünwald S, Performance-based design of self-compacting fibre reinforced concrete, PhD-thesis, TU Delft, 2004.
5. Walraven J, Lehwalter N. Size effects in short beams loaded in shear. *ACI Struct J*. 1994;91(5):583–93.
6. Regan PE. Enhancement of shear resistance in short beams of reinforced concrete, an evaluation of UK recommendations and particularly of BD 44/95. London: University of Westminster; 1998.
7. Walraven JC, Background document for prEN 1002-1-1:2002, Report Delft University of Technology, 25.5-02-36.
8. Droogné D, De Ghein T. Loading tests on high strength fibre reinforced fibre concrete elements. Report, Faculty of Engineering and Architecture. Belgium, Part I: University of Ghent; 2017.
9. König G, Fischer J. Model uncertainties concerning design equations for the shear capacity of concrete members without shear reinforcement. *CEB Bull*. 1995;224:49–100.
10. Taerwe L. Model uncertainties in reliability formats for concrete structures. *CEB Bull*. 1995;224:5–8.
11. RILEM. Bond test for reinforcing steel: 1 beam test. *Mater Struct*. 1970;3(15):169–75.
12. Droogné D, De Ghein T. Loading tests on high strength fibre reinforced fibre concrete elements. Report, Faculty of Engineering and Architecture. Belgium, Part II: University of Ghent; 2018.
13. Li V., Engineered Cementitious Composites, Book 2019, Springer.

## AUTHOR BIOGRAPHIES



**Joost Walraven**, Faculty of Civil Engineering, Delft University of Technology, Delft, The Netherlands.



**Didier Droogné**, Department of Structural Engineering and Building Materials, Ghent University, Ghent, Belgium.



**Steffen Grünwald**, Faculty of Civil Engineering, Delft University of Technology, Delft, The Netherlands; Department of Structural Engineering and Building Materials, Ghent University, Ghent, Belgium.



**Luc Taerwe**, Department of Structural Engineering and Building Materials, Ghent University, Ghent, Belgium; Tongji University, College of Civil Engineering, Shanghai, China.



**Bogdan Cotovanu**, Shell Global Solutions, Rijswijk, The Netherlands.



**John Rovers**, Shell Global Solutions, Rijswijk, The Netherlands.

**How to cite this article:** Walraven J, Droogné D, Grünewald S, Taerwe L, Cotovanu B, Rovers J. Self-compacting high-performance fiber concrete for foundations: Part 1 -experimental verification and design considerations. Structural Concrete. 2021;1–15. <https://doi.org/10.1002/suco.202000440>